

Geophysical Research Letters



RESEARCH LETTER

10.1029/2021GL093152

Key Points:

- Observation of a Terrestrial Electron Beam (TEB) with a spectrum resolved down to 50 keV
- A method to constrain the energy spectrum of the source Terrestrial Gamma ray Flash (TGF) based on the detection of the associated TEB is presented
- Only TGFs originating from fully developed Relativistic Runaway Electron Avalanche models can explain the observation

Supporting Information:

Supporting Information may be found in the online version of this article.

Correspondence to:

D. Sarria,
david.sarria@uib.no

Citation:

Sarria, D., Østgaard, N., Kochkin, P., Lehtinen, N., Mezentsev, A., Marisaldi, M., et al. (2021). Constraining spectral models of a terrestrial gamma-ray flash from a terrestrial electron beam observation by the atmosphere-space interactions monitor. *Geophysical Research Letters*, 48, e2021GL093152. <https://doi.org/10.1029/2021GL093152>

Received 2 MAR 2021

Accepted 14 APR 2021

Constraining Spectral Models of a Terrestrial Gamma-Ray Flash From a Terrestrial Electron Beam Observation by the Atmosphere-Space Interactions Monitor

D. Sarria¹ , N. Østgaard¹ , P. Kochkin¹ , N. Lehtinen¹ , A. Mezentsev¹ , M. Marisaldi¹ , A. Lindanger¹ , C. Maiorana¹ , B. E. Carlson^{1,2} , T. Neubert³ , V. Reglero⁴, K. Ullaland¹ , S. Yang¹ , G. Genov¹ , B. H. Qureshi¹ , C. Budtz-Jørgensen³ , I. Kuvvetli³ , F. Christiansen³ , O. Chanrion³ , J. Navarro-González⁴ , P. Connel⁴, and C. Eyles⁴

¹Birkeland Centre for Space Science, University of Bergen, Bergen, Norway, ²Carthage College, Kenosha, WI, USA,

³National Space Institute, Technical University of Denmark, Lyngby, Denmark, ⁴University of Valencia, Valencia, Spain

Abstract Terrestrial Gamma ray Flashes (TGFs) are short flashes of high energy photons, produced by thunderstorms. When interacting with the atmosphere, they produce relativistic electrons and positrons, and a part gets bounded to geomagnetic field lines and travels large distances in space. This phenomenon is called a Terrestrial Electron Beam (TEB). The Atmosphere-Space Interactions Monitor (ASIM) mounted on-board the International Space Station detected a new TEB event on March 24, 2019, originating from the tropical cyclone Johanina. Using ASIM's low energy detector, the TEB energy spectrum is resolved down to 50 keV. We provide a method to constrain the TGF source spectrum based on the detected TEB spectrum. Applied to this event, it shows that only fully developed Relativistic Runaway Electron Avalanche spectra are compatible with the observation. More specifically, assuming a TGF spectrum $\propto E^{-1} \exp(-E/\epsilon)$, the compatible models have $\epsilon \geq 6.5$ MeV (E is the photon energy and ϵ is the cut-off energy). We could not exclude models with ϵ of 8 and 10 MeV.

Plain Language Summary Terrestrial Gamma ray Flashes (TGF), originating from thunderstorms, are the highest energy natural particle acceleration phenomena occurring on Earth. The production mechanism of TGFs is not well understood. When interacting with the atmosphere, TGFs produce secondary electrons and positrons, and a part gets bounded to Earth's magnetic field lines, and travels large distances in space. They can be detected by instruments on-board satellites located at the right place (in a window of about 40 km) at the right time (in a window of a few milliseconds). This phenomenon is called a Terrestrial Electron Beam (TEB). By detecting the TEB, we can retrieve information about the TGF that produced it. In this article, we present the first TEB originating from a tropical cyclone and with the lowest energies ever recorded (down to 50 keV). We also provide a method to infer properties of the energy distribution of the source TGF (producing the TEB) based on the energy spectrum of the TEB. Applied to this event, it shows that only TGF energy spectra among the most energetic that were proposed are compatible, and we cannot exclude even more energetic events.

1. Introduction

Terrestrial Gamma ray Flashes (TGFs) are short bursts of high energy (<40 MeV) photons, produced during thunderstorms. A review of TGFs theory and observations is presented by Dwyer et al. (2012). TGFs were first detected using the BATSE experiment on-board the CGRO spacecraft (Fishman et al., 1994). Later, TGFs were recorded by the satellites RHESSI (Smith et al., 2005), AGILE (Marisaldi et al., 2014), Fermi (Briggs et al., 2010; Roberts et al., 2018), BeppoSAX (Ursi et al., 2017), and the Atmosphere-Space Interactions Monitor (ASIM) (Neubert, Østgaard, Reglero, Blanc, et al., 2019). ASIM was successfully launched and docked to the International Space Station in April 2018 and started science operations since June 2018. The first results from ASIM were presented by Østgaard, Neubert, et al. (2019); Sarria et al. (2019); Neubert, Østgaard, Reglero, Chanrion, et al. (2019).

When referring to “electrons beams” in the context of TGFs, one can think of two different objects. The first is associated with the production process of the TGF. This production process takes place, at least for TGF detectable from space, between ≈ 10 and ≈ 15 km altitude. This first type of “electron beam” consists of the

© 2021. The Authors.

This is an open access article under the terms of the [Creative Commons Attribution-NonCommercial License](#), which permits use, distribution and reproduction in any medium, provided the original work is properly cited and is not used for commercial purposes.

Relativistic Runaway Electron Avalanche (RREA) producing the TGF's high energy photons. This RREA is not detectable from space since it is impossible for it to go through the atmosphere layer. The second type of "electron beam" is called "terrestrial electron beam" (TEB) and is produced higher in the atmosphere by the TGF's photons, though the processes of Compton scattering and electron-positron pair production. Since electron-positron pair production is involved, TEBs are composed of a fraction of positrons, typically 10%–30% (see Briggs et al. (2011), table 1). A TEB is bound ("beamed") around the magnetic field line intercepting the source TGF's geographical location (Cohen et al., 2010; Dwyer et al., 2008; Sarria et al., 2015). Most electrons and positrons forming TEBs are produced above 40 km altitude, where the air collision frequency of the electrons (and positrons) is comparable to their gyration frequency around geomagnetic field lines. TEBs propagate in space and travel large distances in the magnetosphere. TEBs were first reported from measurements of the CGRO spacecraft (Dwyer et al., 2008). Later, they were detected by Fermi (Briggs et al., 2011; Stanbro et al., 2019), BeppoSAX (Ursi et al., 2017), AGILE (Lindanger et al., 2020), and ASIM (Sarria et al., 2019). RHESSI probably detected one or two TEB event(s), but it has not been 100% confirmed yet (Gjesteland, 2012; Smith et al., 2006). In general, TEBs are detected much less often than TGFs (e.g., Fermi has a few thousand TGFs and about 30 TEBs) because the detector must be located inside a narrow window of less than a few tens of kilometers along the right geomagnetic field line (intercepting the TGF source position), and they last for only a few milliseconds.

One of the reasons of studying TEBs is to retrieve information about the TGFs that produced them. Briggs et al. (2011) constrained the positron fraction to be between 10% and 34%, based on three events. Positron fractions are linked to the spectral shape of the source TGF, as photons with harder spectrums will trigger more electron-positron pair production. In Sarria et al. (2019), the beaming of the source TGF could be constrained between about 30° and 42° (half angle, isotropic within a cone). Another reason to study TEBs is that they may have an impact on the inner Van Allen radiation belt, that has not been quantified yet (to our knowledge). Even if it is an important question, it is not the subject of the present paper.

One of the most important question regarding TGFs is their production mechanism. Two main models are proposed to explain the production of TGFs, and in both, the TGF's photons are produced by high energy electrons through the bremsstrahlung process. These high energy electrons form a RREA (Gurevich et al., 1992; Wilson, 1924). In the first model, a large scale electric field within thunderclouds is considered. This requires the presence of initial high energy seed electrons, that may be provided by cosmic-ray secondaries or background radiation. The background electric field is strong enough to produce RREA avalanches, but the RREA mechanism alone is not enough to produce bright enough TGFs (i.e., detectable from space, therefore, with more than 10^{16} photons between 50 keV and 40 MeV at source), and a x-ray and positron feedback mechanism is required (the "relativistic feedback"); only possible if large potentials are available (Babich et al., 2005; Dwyer, 2012; Dwyer et al., 2003; Skeltved et al., 2014). This mechanism will produce a discharge of the thundercloud that is of different nature than usual lightning discharges. The resulting high-energy photon spectrum given by this model is a so-called "fully developed" RREA. The development of a RREA process can be characterized by the number of avalanche lengths that were achieved (that depends on the extend and magnitude of the available electric potential). The energy spectrum of the electrons converges to a standard shape ($\approx \exp(-E/7.3 \text{ MeV})$), which is fully obtained with six or more avalanche lengths, even if the total number of electrons keeps exponentially increasing with the number of avalanche lengths. Another variant of this model uses a lightning leader to push the background (large scale) field above the threshold to trigger the relativistic feedback mechanism (Skeltved et al., 2017).

The second model of TGF production requires a propagating lightning leader. It is sometimes referred as the "leader-streamer" model. It considers that initial seed electrons are produced by the cold runaway mechanism (Gurevich, 1961), happening in the streamer phase or in the leader phase (Celestin & Pasko, 2011; Chanrion et al., 2014; Dwyer, 2008; Köhn & Ebert, 2015; Moss et al., 2006). These energetic seed electrons follow a specific distribution and a fraction of them are then accelerated and multiplied by a larger scale electric field, producing a RREA. The larger scale electric field can be the field induced by the leader and/or a large scale (background) field in the thunderstorm. In principle, leader-based TGF production models do not exclude the possibility of relativistic feedback, that could be more or less important (Skeltved et al., 2017). A parameter that impacts the energy spectrum of emitted photons the most is the potential drop in the leader tip region that is available for the acceleration of energetic electrons. Resulting TGF

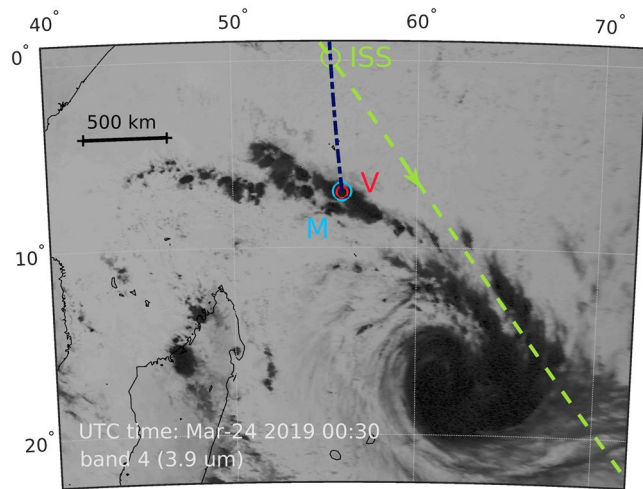


Figure 1. Image from geostationary satellite Meteosat-11 around 00:30 UTC, about 1 min and 53 s before the ASIM trigger. The image comes from the optical band 4 ($3.9 \mu\text{m}$, 3 km resolution). The tropical cyclone Joaninha can be seen in the south-east part of the picture and extends over a thousand of kilometers. The positions of the ISS, the GLD360 match (V), and the magnetic field line footpoint (M) are indicated. The track of the Earth's magnetic field line (dark blue dashed line) and of the trajectory of the ISS (green dashed line) are also showed. Point V is very close to M in both location ($\Delta r = 4.82 \text{ km}$) and time ($\Delta t = 1.44 \text{ m s}$), and is located in the north-western rainbands of the cyclone. ISS, International Space Station.

energy spectra for several leader potential drops are presented in Celestin et al. (2015), figure 3. They actually correspond to a more or less developed RREA process. Celestin et al. (2012) also showed that energy spectra harder than the characteristic fully developed RREA spectrum could be achieved by involving non-equilibrium acceleration of electrons. One significant advantage of leader-based TGF models is that they propose an unified approach to explain TGF's X/gamma ray production, as well as x-ray (i.e., softer) emissions from lightning propagating leaders that were observed from ground, balloons, and aircraft (Dwyer et al., 2003, 2004, 2005, 2011). Mailyan et al. (2019) presented the first study that confronted leader models to TGFs recorded by the Fermi space telescope, with tested potential drops $\leq 200 \text{ MV}$. They found that lightning leader models with potentials of 200 MV and tilted beams gave the best fit to the data in most of the analyzed TGF events. However, the range of compatible models is found to be quite wide.

In this article, we report the second TEB event detected by ASIM on March 24, 2019. Compared to the previous event (presented in Sarria et al. (2019)), data from the two detectors are available: the pixelated Low-Energy detector (50–400 keV) and the High Energy Detector (300 keV–30 MeV), that permits an unprecedented spectral analysis of a TEB event. In Section 2, we present the instruments that were used. In Section 3, we present the event. In Section 4, we present the methods and models we use for the spectral analysis. In Section 5, we show the results of the analysis. We conclude in section 6.

2. Instruments

The ASIM payload (Neubert, Østgaard, Reglero, Blanc, et al., 2019) consists of two main instruments, the Modular X- and Gamma ray Sensor (MXGS) (Østgaard, Balling, et al., 2019) and the Modular Multi-spectral Imaging Array (MMIA) (Chanrion et al., 2019). ASIM is mounted on the International Space Station (ISS) orbiting the Earth at about 400 kms altitude with an inclination of 51.6° . MXGS consists of two detectors for detecting X- and gamma-rays. The MXGS Low-Energy Detector (LED) is layer of 16,384 pixels of Cadmium-Zink-Telluride (CZT) detector crystals, sensitive to photons with energies from 50 keV to about 400 keV. The MXGS High Energy Detector (HED) comprises 12 Bismuth-Germanium-Oxide (BGO) detector modules coupled to photomultiplier tubes (PMT), sensitive in the energy range of 300 keV to about 40 MeV.

GLD360 (VAISALA) is a network of ground-based lightning sensors (1–350 kHz) detecting both Cloud-to-Ground and Intra-Cloud lightning. The GLD360 sensors use a combination of magnetic direction finding and time-of-arrival calculations (from 4 stations or more) to geolocate the lightning source (see acknowledgments for more details). The typical uncertainty on location is about 2.5 km but it can vary a lot with geographical location (Rudlosky et al., 2017).

We also present data provided by the Meteosat-11 geostationary satellite, that provides regular scans of cloud coverage at several wavelengths (used data comes from band 4, at $3.9 \mu\text{m}$, with a 3 km spatial resolution). See acknowledgments for more information.

3. Observation

Figure 1 shows a map of the event together with Satellite imagery that was provided by the geostationary satellite Meteosat-11. The ASIM trigger UTC time is March 24, 2019, 00:31:53.135444 and the ISS was located at latitude of $\phi = 0.157^\circ$, longitude of $\lambda = 55.301^\circ$, and altitude of $h = 408.6 \text{ km}$, that is above the Indian ocean, close to Madagascar. The ASIM clock has a -20 to 30 m s absolute timing uncertainty with respect to GPS UTC time. A VAISALA (GLD360) discharge event with a UTC time of March 24, 2019, 00:31:53.134000

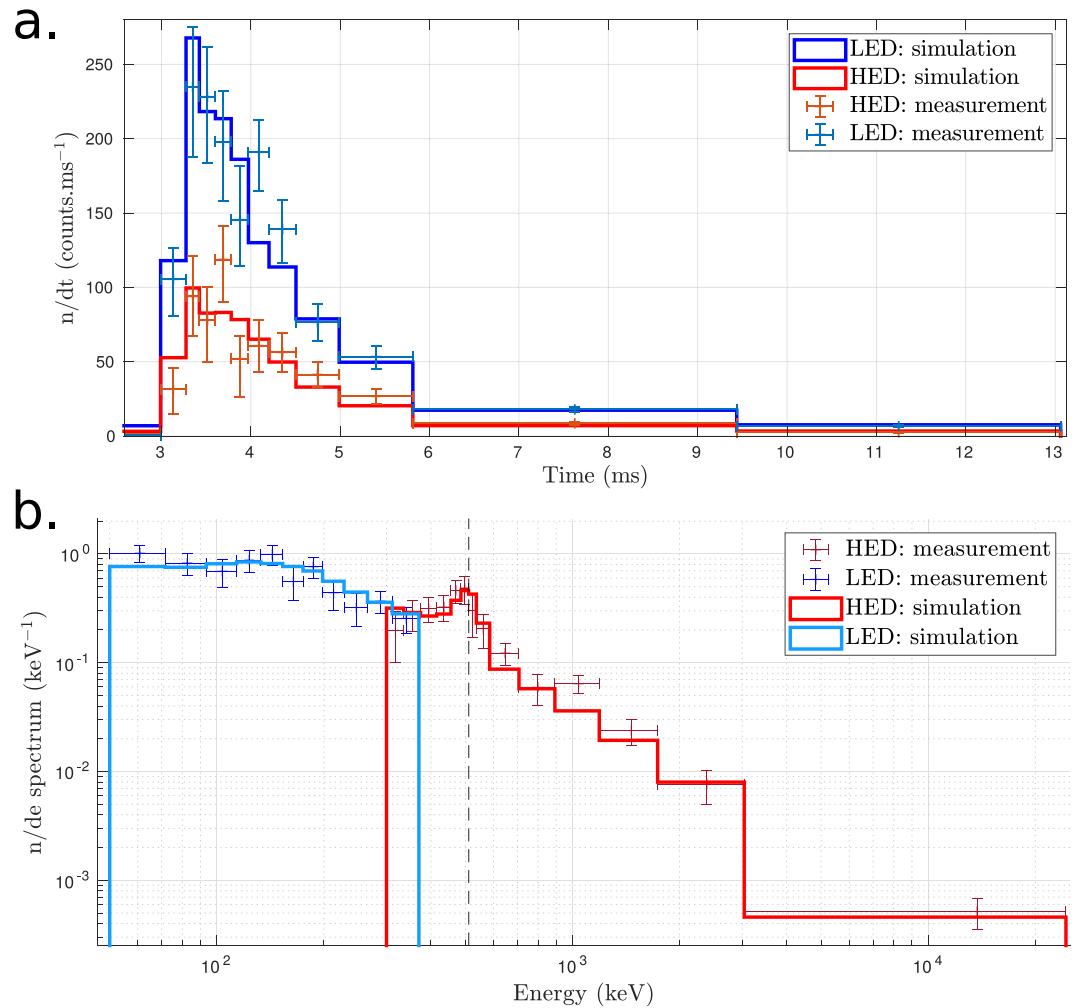


Figure 2. ASIM TEB event 190324. (a) Recorded lightcurve by HED and LED, with 1- σ Poisson error bars. Simulation results from the consensus model are shown and give a good fit to the data ($\chi^2_r(\text{LED})_i = 1.33$, $\chi^2_r(\text{HED})_i = 1.34$). (b) Recorded energy spectrum by HED and LED, with 1- σ Poisson error bars. Simulation results from the consensus model are shown and give a good fit to the data ($\chi^2_e(\text{LED})_e = 0.88$, $\chi^2_e(\text{HED})_e = 0.85$). ASIM, Atmosphere-Space Interactions Monitor; HED, High Energy Detector; LED, Low Energy Detector; TEB, Terrestrial Electron Beam.

($\Delta t = 1.44$ m s) was found very close to the southern magnetic line footprint (at 45 km altitude) intercepting the position of the ISS: [$\phi_{\text{GLD360}} = -7.05^\circ$, $\lambda_{\text{GLD360}} = 55.91^\circ$] and [$\phi_{\text{mag},s} = -7.00^\circ$, $\lambda_{\text{mag},s} = 55.92^\circ$] that gives $\Delta r = 4.82$ km. Note that the GLD360 location uncertainty can be up to 20 km for this event, and the uncertainty in the ISS's position is of the same order. The northern magnetic field line footprint is located at [$\phi_{\text{mag},n} = 20.52^\circ$, $\lambda_{\text{mag},n} = 55.10^\circ$], but no lightning activity was observed close to it. No lightning activity was detected by GLD360 below the ISS, within 540 km and ± 1 s around the trigger time. The MMIA photometers did not detect any lightning activity below the ISS as well.

From satellite imagery (Figure 1), it appears that the southern magnetic field line footprint is located in the rainbands of a tropical cyclone, named “Joaninha.” It is the first time that the detection of a TEB associated to a TGF produced in a cyclone is reported.

Figure 2a shows the recorded lightcurves for LED and HED, as well as a modeling result. The latter is obtained using what will be referred as the “consensus model,” that assumes a source TGF located at the southern magnetic footprint, at 12 km altitude, with an angular distribution following a Gaussian distribution with $\sigma_\theta = 20^\circ$ (centered on zenith), and with an energy spectrum $\propto E^{-1} \exp(-E/7.3 \text{ MeV})$ (maximum energy set to 40 MeV). More information about the modeling is presented in the next section. The consensus

model gives a very good fit to the data (see figure label). Figure 2b shows the spectra recorded by the MXGS instrument for LED and HED. There are a total of 168 recorded counts in HED and 307 counts in LED. The error bars are $1-\sigma$ ($\approx 68\%$ interval) assuming Poisson statistics on the count per bin values given by the model. The spectrum shows a line at 511 keV, that is expected because the electron beams contains a significant fraction of positrons. The consensus model gives a very good fit to the spectral data as well (see figure label), and indicates a positron to electron ratio of 16.1%. This value is comparable to previous results (Briggs et al., 2011).

4. Method to Constrain the Source TGF Spectrum

As presented in the introduction, for any considered TGF production scenario, the spectral shape for the TGF is governed by the RREA process that produces high-energy photons through the bremsstrahlung process. A RREA can be more or less developed depending on how many avalanches lengths have been achieved, that depends on the available potential (in the leader and/or background electric field) and the extend of the electric field(s). The resulting TGF photon energy spectrum can be approximated with Equation 1:

$$f(E) \propto E^{-1} \exp(-E/\epsilon), \text{ with } E < E_m \quad (1)$$

where E is the energy, ϵ is a cut-off energy and E_m is the maximum allowed energy. TGF energy spectra from fully developed RREA are expected to have $\epsilon \geq 5$ MeV (Dwyer, 2012; Sarria et al., 2018; Skeltved et al., 2014). Typical fully developed TGF spectra used in the literature have $\epsilon = 6.5\text{--}7.3$ MeV, and E_m of 30–40 MeV. TGF production models based on a propagating lightning leader can, in theory, produce bright TGFs (i.e., detectable from space, therefore, with more than 10^{16} photons at source) but that shows a partially developed RREA spectrum. This is because, for these models, typically 10^{12} (or more) energetic electrons are initially provided by the cold runaway mechanism. Leader models with potential drops as low as ≈ 160 MV could potentially produce bright TGFs (see Celestin et al. (2015), Table 1). By “potential drop,” it is meant the potential difference between the tip of the lightning leader and the ambient potential.

Equation 1 can fit a fully developed RREA (using $\epsilon \geq 5$ MeV, $E_m = 40$ MeV), as well as partially developed RREA energy spectra resulting from leader models. The leader 300 MV model from Celestin et al. (2015) (figure 3) can be fit by Equation 1 with $\epsilon = 4.7$ MeV and $E_m = 30$ MeV. The 160 MV leader model can be fit by Equation 1 using $\epsilon = 4.3$ MeV and $E_m = 20$ MeV. In the cases of potential drops of 160 and 300 MV, the initial electron's positions are set at 2 and 3.5 m from the leader tip, respectively, because of the shielding of the electric field (Skeltved et al., 2017). The corresponding effective electric potential drops (i.e., that the energetic electrons can use) are, respectively, 28 and 53 MV (Celestin et al., 2015).

In addition to the 160 and 300 MV leader spectra, we chose to test spectra with ϵ equal to 6.5, 7.3, 8, and 10 MeV (all using $E_m = 40$ MeV). The first two values correspond to values used in the literature (Bowers et al., 2017; Dwyer et al., 2012; Sarria et al., 2018; Xu et al., 2019). After looking at the preliminary results using these two values, we decided to add $\epsilon = 8$ MeV and $\epsilon = 10$ MeV. These last two values were primarily added on an ad hoc basis, but a physical justification is that, in theory, non-uniform electric fields in leader models can also produce TGF spectra harder than typical fully developed RREA if non-uniform electric fields are involved (Celestin et al., 2012). We decided not to test values above $\epsilon = 10$ MeV and $E_m = 40$ MeV, since such high energies seem irrelevant for TGFs, given our current undersampling.

To generate a simulated ASIM spectrum, we proceeded to forward modeling of the recorded spectrum, using a two stage simulation. In the first stage, a TGF is started at 12 km altitude, assuming one of the initial energy spectra models, and is propagated to the ISS altitude (about 400 km) using the Geant4-based Monte-Carlo model presented in Sarria et al. (2019) and publicly available (see acknowledgments). Energy, 3D-momentum, and times of electrons/positrons reaching the ISS within a radius of 80 km (at ISS altitude) are saved. At the end of this stage, at least 1 million particle records are required for each tested source TGF spectrum model.

In the second stage, the recorded electrons/positrons are used as input of the ASIM mass model to simulate the response of the instrument. A rotation of frame of reference (Earth to ISS) is applied, and we also included the local geomagnetic field. The used mass model includes the ASIM detectors (MXGS, MMIA),

the instrument platform, as well as non-negligible surrounding elements (e.g., the Columbus module). The energy deposition on the detectors can be direct, that is, electrons/positrons hitting directly a CZT or BGO crystal, or indirect. In the indirect case, electrons/positrons emit bremsstrahlung photons by interaction with the surrounding material that hit at least one crystal. Photons can also come from annihilating positrons, with specific energy of 511 keV. For HED, because of the shielding, about 98% of the energy deposition is due to indirect hits into the BGO crystals. For LED, direct hits are more important: about 72% of the energy deposition. This explains why the effective area of LED is larger than HED when considering incident electrons/positrons. The effective area is calculated as the geometrical area ($\approx 900 \text{ cm}^2$ for HED and $\approx 1,024 \text{ cm}^2$ for LED) multiplied by the probability of an incident TEB electron to deposit more than 300 keV into at least one BGO crystal (for HED), or more than 50 keV into at least one CZT pixel (for LED).

At the end of the second stage, a simulation data set in the form of a list of detected time and energy counts is generated. To be able to completely neglect the simulation noise, it is required to have at least 1,000,000 counts on each detector to build each energy spectrum and calculate the effective areas. The final modeled spectra also include a background component build from real background data.

A key feature of performing spectral analysis on the TEB, instead of TGF, is that the energy spectrum of the constituting electrons and positrons above 100 km altitude is only weakly dependent on the following parameters:

- the radial distance between the TEB center and the ISS. The concept of radial is presented more precisely in the supporting information, Figure A.1
- the beaming and the tilt angles of the source TGF
- the source altitude of the TGF, if set between 10 and 15 km

Actually, we found that the spectrum of the source TGF is the dominating factor that affects the spectrum of the detected TEB. This permit a substantial simplification of the problem as it reduces drastically the number of free parameters to include in the analysis. Since these three points are crucial for this analysis, we provide in the supporting information document more detailed arguments and simulation results supporting those three points. It includes the results of the procedure described below if applied to source TGF altitudes of 10 and 15 km, and various opening angle distributions and tilt angles. The effect of the source TGF altitude is small and does not affect significantly the results presented next (this issue discussed into details in the supporting information, section B). In the following, we fix the source TGF model to a source altitude to 12 km, a Gaussian angular distribution with $\sigma = 20^\circ$, and no tilt angle.

The simulated spectra are evaluated with respect to the observation, separately for the LED (50–370 keV) and the HED (0.3–40 MeV), and with both detectors together. To compare the modeling results to the observation, we use three methods: a likelihood analysis, a χ^2 analysis (Eadie et al., 1971; Lyons, 1986; Martin, 1971), and the effective LED/HED area ratio. Note that these three criteria are not independent as they use the same data sets: the list of measured and simulated energy counts by the HED and the LED.

For the likelihood analysis, a value of $-2\ln(\mathcal{L})$, the Negative Log-Likelihood, is calculated. The model with the lowest value of $-2\ln(\mathcal{L})$ is considered to be the best description of the observation. Models are considered to be also possible if their $-2\ln(\mathcal{L})$ values have a difference of less than a threshold value τ . We calculated that $\tau \approx 5$ for a confidence level of about 99%, similar to the one used by Mailyan et al. (2016) for Fermi-GBM observations. This value assumes that $-2\ln(\mathcal{L})$ evolves following approximately a normal distribution with respect to the free parameter(s). In the following, we present the values Δ_{mle} , that are the values of $-2\ln(\mathcal{L})$ subtracted by the value of $-2\ln(\mathcal{L})$ for the best model. Therefore, the best model has $\Delta_{mle} = 0$ and compatible models have $\Delta_{mle} \leq \tau$. A verification if a given model was found worse than another just because of random fluctuations (“by chance”) is also performed.

We also provide a reduced χ^2 value, noted χ_r^2 . If χ_r^2 is below a critical value, the model is considered compatible with the measurement, and above the model is considered incompatible. The Pearson’s χ^2 method is affected by choice of binning (i.e., energy intervals chosen to build the spectra). To mitigate this effect, we chose a binning with at least 7 measurement counts on each bin for HED, and at least 10 for LED. These two binnings are used to make the spectra presented in Figure 2b. Given the used binning, the critical value

Table 1
Table Summarizing the Comparison of the Tested Spectral Models With the Measurement

Model	Effective area in cm ²			Maximum likelihood analysis result value Δ_{mle}			Pearson's χ_r^2			e^+/e^- ratio
	LED	HED	LED/HED effective area ratio	LED	HED	Co.	LED	HED	Co.	
“Leader 160 MV” $\epsilon = 4.3$ MeV $E_m = 19.2$ MeV	122.0	43.7	2.79	0	19.0	22.5	0.84	1.97	1.66	10.3%
“Leader 300 MV” $\epsilon = 4.7$ MeV $E_m = 32$ MeV	141.5	61.0	2.32	0	3.4	7.1	0.88	1.04	1.31	13.3%
$\epsilon = 6.5$ MeV $E_m = 40$ MeV	156.0	74.4	2.10	0.2	0.8	3.1	0.89	0.87	1.27	15.2%
$\epsilon = 7.3$ MeV $E_m = 40$ MeV	162.2	80.4	2.02	0.3	0.2	1.9	0.88	0.85	1.28	16.1%
$\epsilon = 8$ MeV $E_m = 40$ MeV	168.4	85.5	1.97	0.5	0	1.1	0.89	0.84	1.29	16.8%
$\epsilon = 10$ MeV $E_m = 40$ MeV	177.8	94.7	1.88	0.5	1.0	0	0.90	0.83	1.30	18.3%
Compatibility range	n.a.		1.82 ± 0.35		≤ 5		≤ 1.94	≤ 1.75	≤ 1.57	

Three main criteria are presented: the led/hed effective area ratio, the maximum likelihood and the Pearson's χ_r^2 . “Co.” stands for the led and hed combination. the compatibility range for the different criteria are also indicated. bold values indicate compatible models for the given criteria (column).
Abbreviations: HED, High Energy Detector; LED, Low Energy Detector.

$\chi_{r,c}^2$ is 1.94 (8 degrees of freedom) for the LED, 1.75 for the HED (12 degrees of freedom), and 1.57 for the combination of both (20 degrees of freedom).

Compared to the Pearson's χ^2 , the maximum likelihood analysis presents the advantage of not relying on a binning of the measurement data: it keeps all its granularity, that is, no information is lost by binning the measurements. The maximum likelihood analysis is better suited than the χ^2 to estimate which model is the best description of the observation (see, e.g., Hauschild & Jentschel, 2001)

5. Results and Discussion

Table 1 summarizes the results of this study. The models are sorted according the prevalence of high energies (also called “hardness”) or, equivalently, by decreasing LED/HED effective area ratio. As indicated in the previous section, three main evaluation criteria are presented: the reduced Pearson's χ_r^2 , the maximum likelihood, and the LED/HED effective area ratio.

Concerning the LED spectral fits (Table 1), all the models give good fits, using the χ_r^2 or the Maximum likelihood analysis. We interpret this as the energy range of 50–370 keV being too narrow to discriminate between the models.

Concerning the HED spectral fits, looking at the χ_r^2 values, only the 160 MV leader model is found incompatible. This criterion gives similar conclusions when LED and HED spectra are combined.

The maximum likelihood analysis on the HED spectrum shows that the best model is for $\epsilon = 8$ MeV. The fit for $\epsilon = 7.3$ MeV is also very close. It indicates that the leader 300 MV model and harder spectra are also possible explanations. If LED and HED spectra are combined, the best model is then $\epsilon = 10$ MeV (but $\epsilon = 8$ MeV is a very close fit), and only models with $\epsilon = 6.5$ MeV or greater are compatible.

Since 307 counts are observed for LED (>50 keV) and 168 for HED (>300 keV), the observed ratio is 1.83. Considering that the two count numbers individually follow a Poisson statistic (but the ratio does not), the uncertainty on the ratio is ± 0.35 (95% interval). It implies that, using this criterion, the two leader-based source TGF spectral models (160 and 300 MV) are incompatible. The effective area ratio analysis indicates that the models with $\epsilon \geq 6.5$ MeV are compatible. In particular, we cannot exclude $\epsilon = 8$ and $\epsilon = 10$ MeV. This is a similar result as obtained with the maximum likelihood analysis.

For this event, TGF spectra harder than previously expected are not excluded. AGILE did report observations of TGF surprisingly hard (up to 100 MeV), but they were later found explainable from instrumental effects (Marisaldi et al., 2019). Our analysis does not exclude that the mechanism presented in (Celestin et al., 2012) could not be responsible for producing TGFs with a slightly harder energy spectra than fully developed RREA.

The results presented in this article are only valid for a single event, and it does not imply that leader models with potentials of 300 MV or less could explain other TGF (and TEB) events. It is also possible that because our method relies on the detection of a TEB, we are biased toward a population of strong TGFs, necessitating fully developed RREAs. TGFs that could originate from non-fully-developed RREAs (leader models) may never (or very rarely) produce a detectable TEB. This question could be addressable in the future, by applying this analysis to more TEB events. We list possibilities of new studies in the next section.

Finally, Table 1 also indicates the positron/electron ratio. The model giving the best fit ($\epsilon = 10$ MeV) gives a ratio of 18.3%, and the range of compatible models give a ratio ranging from 15.2% to 18.3%. This range is compatible with estimations from the Fermi space telescope team (Briggs et al., 2011).

6. Conclusions and Future Work

We reported the observation of a Terrestrial Electron Beam by ASIM on March 24, 2019, originating from the rainbands of the tropical cyclone Johanina. The associated lightning stroke was detected by the GLD360 network (VAISALA) in close temporal association and very close to the ISS's south magnetic field line footpoint. The TEB spectrum was resolved down to 50 keV for the first time, using the low energy detector (LED) of ASIM. A method to constrain the TGF source energy spectrum based on the TEB detection was presented. It relies on a reduction of the number of free parameters (altitude, angular distribution, and radial distance) possible due to TEB's properties. Comprehensive Monte Carlo simulations were performed to reproduce the observation, assuming several energy spectrum shapes of the source TGF. Using three criteria to evaluate the simulation results with respect to the observation (Maximum likelihood, Pearson's χ_r^2 and LED/HED count ratio), we showed that source TGF with, at least, a fully developed RREA spectrum $\propto E^{-1} \exp(-E/\epsilon)$ (with $\epsilon \geq 6.5$ MeV, $E_m = 40$ MeV) is compatible with the observation. We could not exclude harder models with $\epsilon = 8$ MeV ($E_m = 40$ MeV) and 10 MeV ($E_m = 40$ MeV), that could potentially be explained by non-equilibrium acceleration of energetic electrons in lightning (Celestin et al., 2012).

In the future, we expect that a larger number of events will be processed using the method presented in this article. For ASIM, it will not be possible before several more years of data gathering, since it currently detects about 4 TEB a year, and not all of them present LED data (only turned ON during the night time of the ISS) or enough counts on LED and HED. In principle, the method presented in this article could also be applied/translated to events from the Fermi GBM TGF/TEB catalog (Roberts et al., 2018), that currently contains about 30 TEB events. Fermi GBM has and high energy (BGO-based) detectors that covers an energy range of ≈ 150 keV to ≈ 30 MeV. GBM's NaI detectors could also be used in principle (with an energy range of a few keV to 1 MeV) but no TEB spectrum using it was reported yet. Since TEB events present lower fluxes (counts per second) than TGFs (typically 20 times), it makes the spectral analysis much less challenging than for TGF events: instrumental effects (dead-time, pile-up), affecting TGF analysis, can be mostly (if not totally) ignored for TEB spectral analysis.

Data Availability Statement

The data presented in this article is available in the following Zenodo repository: <https://doi.org/10.5281/zenodo.4264459>.

The Geant4-based model for Terrestrial Gamma ray Flash (TGF) and associated electrons and positrons propagation in Earth atmosphere and environment (magnetic field) is available in the following repository: <https://doi.org/10.5281/zenodo.2597039>.

Acknowledgments

This work was supported by the European Research Council under the European Union's Seventh Framework Program (FP7/2007–2013)/ERC grant agreement n. 320839 and the Research Council of Norway under contract 223252/F50 (CoE). ASIM is a mission of ESA's SciSpace Program for scientific utilization of the ISS and non-ISS space exploration platforms and space environment analogs. This study has received funding from the European Union's Horizon 2020 research and innovation program under the Marie Skłodowska-Curie grant agreement SAINT 722337. ASIM was funded through the ESA ELIPS program, through contracts with TERMA and Danish Technical University (DTU) in Denmark, University of Bergen (UB) in Norway and University of Valencia (UV) in Spain. Additional funding was supported by the ESA PRODEX contracts PEA 4000105639 and 4000111397 to DTU and ESA PRODEX contract 4000102100 and by Norwegian Research Council to UB. The ASIM Science Data Center (ASDC) at DTU is supported by PRODEX contract PEA 4000115884 and by PRODEX contract PEA4000123438 at UB. The ASIM Science Data Center and data analysis activities at the UV are supported by the MINECO Research Grants ESP2015- 69909-C5-1-R and ESP2017-86263-C4-1-R. The authors thank Vaisala Inc. for access to the GLD360 data. For more information, see <https://www.vaisala.com/en/products/systems/lightning/gld360>. The authors acknowledge EUMETSAT for making accessible images from the Meteosat-11 geostationary satellite and the MCFETCH service (<https://mcfetch.ssec.wisc.edu/>) from the Satellite Data Services (SDS) group, at the University of Wisconsin-Madison Space Science and Engineering Center (SSEC), that is responsible for the access, maintenance, and distribution of real-time and archive weather satellite data. The simulations were performed on resources provided by UNINETT Sigma2 – the National Infrastructure for High Performance Computing and Data Storage in Norway, under project no. NN9526K.

References

- Babich, L. P., Donskoy, E. N., Kutsyk, I. M., & Roussel-Dupré, R. A. (2005). The feedback mechanism of runaway air breakdown. *Geophysical Research Letters*, 32(9). <https://doi.org/10.1029/2004GL021744>
- Bowers, G. S., Smith, D. M., Martinez-McKinney, G. F., Kamogawa, M., Cummer, S. A., Dwyer, J. R., et al. (2017). Gamma ray signatures of neutrons from a terrestrial gamma ray flash. *Geophysical Research Letters*, 44(19). <https://doi.org/10.1002/2017GL075071>
- Briggs, M. S., Connaughton, V., Wilson-Hodge, C., Preece, R. D., Fishman, G. J., Kippen, R. M., et al. (2011). Electron-positron beams from terrestrial lightning observed with Fermi GBM. *Geophysical Research Letters*, 38, L02808. <https://doi.org/10.1029/2010GL046259>
- Briggs, M. S., Fishman, G. J., Connaughton, V., Bhat, P. N., Paciesas, W. S., Preece, R. D., et al. (2010). First results on terrestrial gamma ray flashes from the fermi gamma-ray burst monitor. *Journal of Geophysical Research*, 115, A07323. <https://doi.org/10.1029/2009JA015242>
- Celestin, S., & Pasko, V. P. (2011). Energy and fluxes of thermal runaway electrons produced by exponential growth of streamers during the stepping of lightning leaders and in transient luminous events. *Journal of Geophysical Research*, 116, A03315. <https://doi.org/10.1029/2010JA016260>
- Celestin, S., Xu, W., & Pasko, V. P. (2012). Terrestrial gamma ray flashes with energies up to 100 MeV produced by nonequilibrium acceleration of electrons in lightning. *Journal of Geophysical Research*, 117(A5). <https://doi.org/10.1029/2012JA017535>
- Celestin, S., Xu, W., & Pasko, V. P. (2015). Variability influence and spectrum of high-energy photon bursts produced by lightning leaders. *Journal of Geophysical Research: Space Physics*, 120(12), 10,712–10,710. <https://doi.org/10.1002/2015JA021410>
- Chanrion, O., Bonaventura, Z., Çinar, D., Bourdon, A., & Neubert, T. (2014). Runaway electrons from a 'beam-bulk' model of streamer: Application to TGFs. *Environmental Research Letters*, 9(5), 055003. <https://doi.org/10.1088/1748-9326/9/5/055003>
- Chanrion, O., Neubert, T., Lundgaard Rasmussen, I., Stoltze, C., Tcherniak, D., Jessen, N. C., et al. (2019). The Modular Multispectral Imaging Array (MMIA) of the ASIM payload on the international space station. *Space Science Reviews*, 215, 28. <https://doi.org/10.1007/s11214-019-0593-y>
- Cohen, M. B., Inan, U. S., Said, R. K., Briggs, M. S., Fishman, G. J., Connaughton, V., & Cummer, S. A. (2010). A lightning discharge producing a beam of relativistic electrons into space. *Geophysical Research Letters*, 37(18), L18806. <https://doi.org/10.1029/2010GL044481>
- Dwyer, J. R. (2008). Source mechanisms of terrestrial gamma-ray flashes. *Journal of Geophysical Research*, 113(D10), D10103. <https://doi.org/10.1029/2007JD009248>
- Dwyer, J. R. (2012). The relativistic feedback discharge model of terrestrial gamma ray flashes. *Journal of Geophysical Research*, 117(A2), A02308. <https://doi.org/10.1029/2011JA017160>
- Dwyer, J. R., Grefenstette, B. W., & Smith, D. M. (2008). High-energy electron beams launched into space by thunderstorms. *Geophysical Research Letters*, 35, L02815. <https://doi.org/10.1029/2007GL032430>
- Dwyer, J. R., Rassoul, H. K., Al-Dayeh, M., Caraway, L., Chrest, A., Wright, B., et al. (2005). X-ray bursts associated with leader steps in cloud-to-ground lightning. *Geophysical Research Letters*, 32(1). <https://doi.org/10.1029/2004gl021782>
- Dwyer, J. R., Rassoul, H. K., Al-Dayeh, M., Caraway, L., Wright, B., Chrest, A., et al. (2004). Measurements of X-ray emission from rocket-triggered lightning. *Geophysical Research Letters*, 31(5). <https://doi.org/10.1029/2003gl018770>
- Dwyer, J. R., Schaal, M., Rassoul, H. K., Uman, M. A., Jordan, D. M., & Hill, D. (2011). High-speed X-ray images of triggered lightning dart leaders. *Journal of Geophysical Research*, 116(D15), D20208. <https://doi.org/10.1029/2011JD015973>
- Dwyer, J. R., Smith, D. M., & Cummer, S. A. (2012). High-energy atmospheric physics: Terrestrial gamma-ray flashes and related phenomena. *Space Science Reviews*, 173(1–4), 133–196. <https://doi.org/10.1007/s11214-012-9894-0>
- Dwyer, J. R., Uman, M. A., Rassoul, H. K., Al-Dayeh, M., Caraway, L., Jerauld, J., et al. (2003). Energetic radiation produced during rocket-triggered lightning. *Science*, 299, 694–697. <https://doi.org/10.1126/science.1078940>
- Eadie, W. T., Drijard, D., James, F. R., Roos, M., & Sadoulet, B. (1971). *Statistical methods in experimental physics*. Amsterdam, North-Holland. Retrieved from <https://cds.cern.ch/record/100342>
- Fishman, G. J., Bhat, P. N., Mallozzi, R., Horack, J. M., Koshut, T., Kouveliotou, C., et al. (1994). Discovery of intense gamma-ray flashes of atmospheric origin. *Science*, 264(5163), 1313–1316. <https://doi.org/10.1126/science.264.5163.1313>
- Gjesteland, T. (2012). *Properties of terrestrial gamma ray flashes. Modeling and analysis of BATSE and RHESSI data (PhD thesis)*, The University of Bergen. Retrieved from <http://bora.uib.no/handle/1956/6203>
- Gurevich, A. V. (1961). On the theory of runaway electrons. *Soviet Physics Journal of Experimental and Theoretical Physics*, 12(5), 904–912.
- Gurevich, A. V., Milikh, G. M., & Roussel-Dupré, R. (1992). Runaway electron mechanism of air breakdown and preconditioning during a thunderstorm. *Physics Letters A*, 165(5–6), 463–468. [https://doi.org/10.1016/0375-9601\(92\)90348-p](https://doi.org/10.1016/0375-9601(92)90348-p)
- Hauschild, T., & Jentschel, M. (2001). Comparison of maximum likelihood estimation and chi-square statistics applied to counting experiments. *Nuclear Instruments and Methods in Physics Research Section A: Accelerators, Spectrometers, Detectors and Associated Equipment*, 457(1), 384–401. [https://doi.org/10.1016/S0168-9002\(00\)00756-7](https://doi.org/10.1016/S0168-9002(00)00756-7). Retrieved from <http://www.sciencedirect.com/science/article/pii/S0168900200007567>
- Köhn, C., & Ebert, U. (2015). Calculation of beams of positrons, neutrons, and protons associated with terrestrial gamma ray flashes. *Journal of Geophysical Research - D: Atmospheres*, 120(4), 1620–1635. <https://doi.org/10.1002/2014JD022229>
- Lindanger, A., Marisaldi, M., Maiorana, C., Sarria, D., Albrechtsen, K., Østgaard, N., et al. (2020). The 3rd AGILE terrestrial gamma ray flash catalog. Part I: Association to lightning sferics. *Journal of Geophysical Research - D: Atmospheres*, 125(11), e2019JD031985. <https://doi.org/10.1029/2019JD031985>
- Lyons, L. (1986). *Statistics for nuclear and particle physicists*. <https://doi.org/10.1017/cbo9781139167710>
- Mailyan, B. G., Briggs, M. S., Cramer, E. S., Fitzpatrick, G., Roberts, O. J., Stanbro, M., et al. (2016). The spectroscopy of individual terrestrial gamma-ray flashes: Constraining the source properties. *Journal of Geophysical Research: Space Physics*, 121(A10), 346, 11. <https://doi.org/10.1002/2016JA022702>
- Mailyan, B. G., Xu, W., Celestin, S., Briggs, M. S., Dwyer, J. R., Cramer, E. S., et al. (2019). Analysis of individual terrestrial gamma-ray flashes with lightning leader models and fermi gamma-ray burst monitor data. *Journal of Geophysical Research: Space Physics*, 124(8), 7170–7183. <https://doi.org/10.1029/2019ja026912>. Retrieved from <https://agupubs.onlinelibrary.wiley.com/doi/abs/10.1029/2019JA026912>

- Marisaldi, M., Fuschino, F., Tavani, M., Dietrich, S., Price, C., Galli, M., et al. (2014). Properties of terrestrial gamma ray flashes detected by AGILE MCAL below 30 MeV. *Journal of Geophysical Research: Space Physics*, 119, 1337–1355. <https://doi.org/10.1002/2013JA019301>
- Marisaldi, M., Galli, M., Labanti, C., Østgaard, N., Sarria, D., Cummer, S. A., et al. (2019). On the High-Energy Spectral Component and Fine Time Structure of Terrestrial Gamma Ray Flashes. *Journal of Geophysical Research - D: Atmospheres*, 124(14), 7484–7497. <https://doi.org/10.1029/2019jd030554>. Retrieved 2021-01-22, from <https://onlinelibrary.wiley.com/doi/abs/10.1029/2019JD030554>
- Martin, B. R. (1971). *Statistics for physicists [by] B. R. Martin*. Academic Press London, New York.
- Moss, G. D., Pasko, V. P., Liu, N., & Veronis, G. (2006). Monte Carlo model for analysis of thermal runaway electrons in streamer tips in transient luminous events and streamer zones of lightning leaders. *Journal of Geophysical Research*, 111, 2307. <https://doi.org/10.1029/2005JA011350>
- Neubert, T., Østgaard, N., Reglero, V., Blanc, E., Chanrion, O., Oxborrow, C. A., et al. (2019). The ASIM mission on the international space station. *Space Science Reviews*, 215(2), 26. <https://doi.org/10.1007/s11214-019-0592-z>. Retrieved 2021-01-22, from <http://link.springer.com/10.1007/s11214-019-0592-z>
- Neubert, T., Østgaard, N., Reglero, V., Chanrion, O., Heumesser, M., Dimitriadou, K., et al. (2019). A terrestrial gamma-ray flash and ionospheric ultraviolet emissions powered by lightning. *Science*, 367, 183, 186, eaax3872. Retrieved 2021-01-20, from <https://doi.org/10.1126/science.aax3872>
- Østgaard, N., Balling, J. E., Bjørnsen, T., Brauer, P., Budtz-Jørgensen, C., Buijwan, W., et al. (2019). The Modular X- and Gamma-Ray Sensor (MXGS) of the ASIM payload on the international space station. *Space Science Reviews*, 215, 23. <https://doi.org/10.1007/s11214-018-0573-7>
- Østgaard, N., Neubert, T., Reglero, V., Ullaland, K., Yang, S., Genov, G., et al. (2019). First 10 Months of TGF Observations by ASIM. *Journal of Geophysical Research - D: Atmospheres*, 124(24), 14024–14036. <https://doi.org/10.1029/2019jd031214>. Retrieved 2021-01-20, from <https://onlinelibrary.wiley.com/doi/10.1029/2019JD031214>
- Roberts, O. J., Fitzpatrick, G., Stanbro, M., McBreen, S., Briggs, M. S., Holzworth, R. H., et al. (2018). The first fermi -GBM terrestrial gamma ray flash catalog. *Journal of Geophysical Research: Space Physics*, 123, 4381–4401. <https://doi.org/10.1029/2017JA024837>
- Rudlosky, S. D., Peterson, M. J., & Kahn, D. T. (2017). GLD360 Performance Relative to TRMM LIS. *Journal of Atmospheric and Oceanic Technology*, 34(6), 1307–1322. <https://doi.org/10.1175/JTECH-D-16-0243.1>
- Sarria, D., Blelly, P.-L., & Forme, F. (2015). MC-PEPTITA: A Monte Carlo model for photon, electron and positron tracking in terrestrial atmosphere-application for a terrestrial gamma ray flash. *Journal of Geophysical Research: Space Physics*, 120(5), 3970–3986. <https://doi.org/10.1002/2014ja020695>. Retrieved from <https://agupubs.onlinelibrary.wiley.com/doi/abs/10.1002/2014JA020695>
- Sarria, D., Kochkin, P., Østgaard, N., Lehtinen, N., Mezentsev, A., Marisaldi, M., et al. (2019). The first terrestrial electron beam observed by the atmosphere-space interactions monitor. *Journal of Geophysical Research: Space Physics*, 124(12), 10497–10511. <https://doi.org/10.1029/2019JA027071>
- Sarria, D., Rutjes, C., Diniz, G., Luque, A., Ihaddadene, K. M. A., Dwyer, J. R., et al. (2018). Evaluation of Monte Carlo tools for high-energy atmospheric physics II: Relativistic runaway electron avalanches. *Geoscientific Model Development*, 11, 4515–4535. <https://doi.org/10.5194/gmd-11-4515-2018>
- Skeltved, A. B., Østgaard, N., Carlson, B., Gjesteland, T., & Celestin, S. (2014). Modeling the relativistic runaway electron avalanche and the feedback mechanism with GEANT4. *Journal of Geophysical Research: Space Physics*, 119, 9174–9191. <https://doi.org/10.1002/2014JA020504>
- Skeltved, A. B., Østgaard, N., Mezentsev, A., Lehtinen, N., & Carlson, B. (2017). Constraints to do realistic modeling of the electric field ahead of the tip of a lightning leader. *Journal of Geophysical Research - D: Atmospheres*, 122(15), 8120–8134. <https://doi.org/10.1002/2016jd026206>. Retrieved from <https://agupubs.onlinelibrary.wiley.com/doi/abs/10.1002/2016JD026206>
- Smith, D. M., Grefenstette, B. W., Splitt, M., Lazarus, S. M., Rassoul, H. K., Coleman, L. M., et al. (2006). *The anomalous terrestrial gamma-ray flash of 17 January 2004*. AGU Fall Meeting Abstracts, AE31A–1040.
- Smith, D. M., Lopez, L. I., Lin, R. P., & Barrington-Leigh, C. P. (2005). Terrestrial gamma-ray flashes observed up to 20 MeV. *Science*, 307, 1085–1088. <https://doi.org/10.1126/science.1107466>
- Stanbro, M., Briggs, M. S., Roberts, O. J., Cramer, E., Dwyer, J. R., Holzworth, R. H., et al. (2019). A fermi gamma-ray burst monitor event observed as a terrestrial gamma-ray flash and terrestrial electron beam. *Journal of Geophysical Research: Space Physics*, 124(12), 10580–10591. <https://doi.org/10.1029/2019ja026749>. Retrieved from <https://agupubs.onlinelibrary.wiley.com/doi/abs/10.1029/2019JA026749>
- Ursi, A., Guidorzi, C., Marisaldi, M., Sarria, D., & Frontera, F. (2017). Terrestrial gamma-ray flashes in the BeppoSAX data archive. *Journal of Atmospheric and Solar-Terrestrial Physics*, 156, 50–56. <https://doi.org/10.1016/j.jastp.2017.02.014>
- Wilson, C. T. R. (1924). The electric field of a thundercloud and some of its effects. *Proceedings of the Physical Society, London*, 37, 32D–37D. <https://doi.org/10.1088/1478-7814/37/1/314>
- Xu, W., Celestin, S., Pasko, V. P., & Marshall, R. A. (2019). Compton Scattering Effects on the Spectral and Temporal Properties of Terrestrial Gamma-Ray Flashes. *Journal of Geophysical Research: Space Physics*, 124(8), 7220–7230. <https://doi.org/10.1029/2019ja026941>. Retrieved from <https://agupubs.onlinelibrary.wiley.com/doi/abs/10.1029/2019JA026941>